TRACKING SYSTEM FOR A PARABOLIC DISH SOLAR CONCENTRATOR: DEVELOPMENT AND EVALUATION

Marco Damasceno de Sousa[1], Adriano da Silva Marques[2], João Pedro Cruz de Almeida[3], Leonardo Pereira de Lucena Silva[4]

[1,3] Postgraduate degree in renewable energies, Center for Alternative and Renewable Energies, Federal University of Paraíba, João Pessoa (Brazil)

[2] Department of Renewable Energy Engineering, Center for Alternative and Renewable Energy, Federal University of Paraíba, João Pessoa(Brazil).

[1,4] Professor at the Federal Institute of Paraíba IFPB, Industrial unit, Cajazeiras (Brazil).

Abstract

This work presents the development and evaluation of a two-axis active solar tracking system applied to a parabolic dish solar concentrator (CSP). The objective was to ensure higher accuracy in aligning the concentrator with the Sun's position, thereby maximizing the capture of Direct Normal Irradiance (DNI). The system employs paired LDR sensors connected to an Arduino microcontroller, which implements a control algorithm with a function called *rampPWM*, designed to smooth motor actuation and reduce mechanical stress. The methodology included hourly measurements of DNI and Global Horizontal Irradiance (GHI), as well as the determination of the Instantaneous Solar Tracking Error (ISTE) using a gnomon. The system was experimentally tested over a period of 10 days. Results indicated that, on clear-sky days, DNI exceeded GHI by up to 64%, while on partly cloudy days the gain was reduced. The maximum ISTE recorded during the tests was 2.86°, demonstrating the good performance of the tracker. It can be concluded that the system is robust, efficient, and shows potential for application in both CSP solar technologies and photovoltaic systems.

Keywords: *Solar tracker, accuracy, solar concentrator, solar energy, automation, solar radiation.*

1. Introduction

Solar tracking mechanisms play a key role in maximizing the efficiency of solar energy systems, being applicable to both photovoltaic modules and concentrating technologies, such as parabolic dish concentrator systems (CSP). In the specific case of CSP systems, tracking accuracy is a critical factor, since these devices operate exclusively with direct normal irradiance (DNI), which is concentrated onto a focal point known as the receiver or energy absorber (Stanek et al., 2022).

Solar trackers can be classified according to the number of movement axes. Single-axis models follow the Sun's azimuthal trajectory, whereas dual-axis trackers account for both the azimuthal path and the variation of the solar elevation angle (Kuttybay et al., 2024). They can also be classified as passive or active trackers. Active systems employ sensors, actuators, and controllers to continuously adjust the position, while passive trackers rely on materials with thermal or mechanical properties, such as thermal expansion fluids, which move in response to solar heating (Kuttybay et al., 2024). An example of a purely mechanical passive tracker is presented by Elsayed et al. (2021).

10.18086/swc.2025.06.33 Available at http://proceedings.ises.org

Moreover, active trackers differ according to the control strategies adopted, which can be classified into open-loop or closed-loop systems (Al-Saadi et al., 2022). In open-loop systems, positioning is adjusted based on predefined mathematical models that take into account parameters such as geographic location, date, and time. In contrast, closed-loop systems employ sensors that provide real-time information to a controller, which continuously adjusts the solar tracker's position, ensuring higher accuracy in capturing solar radiation (Hammoumi et al., 2022).

Several solar tracking systems have been designed and evaluated in recent years. Al-Saadi et al. (2022) developed a dual-axis tracking system based on a mathematical model integrated with a microcontroller, a global positioning system (GPS), and a gyroscope, enabling the system to be used anywhere in the world.

Researchers tested a tracking prototype on a small photovoltaic module based on analog components, employing a Wheatstone bridge, operational amplifiers, and LDR sensors (Saeedi & Effatnejad, 2021). Energy production was compared with a fixed module, and a gross energy gain of 48.2% was observed. However, this method requires constant balancing and calibration, as well as a larger number of circuits and connections. More recently, Sun et al. (2024) developed and tested a single-axis solar tracking method for bifacial photovoltaic modules based on an adaptive tracking algorithm. The results demonstrated that the algorithm increased the energy yield by 32.7% on the front side and 7.5% on the rear side.

Queiroz et al. (2020) proposed a dual-axis solar tracking prototype applied to photovoltaic modules, using LDR sensors arranged in four quadrants. The authors reported a 39.5% increase in total generated energy and a net gain of 32.16% compared to a fixed system. Similarly, Sousa et al. (2022) developed an active single-axis tracker, analyzed in the Brazilian context (article in Portuguese), which achieved a net energy gain of 22.81% on clear-sky days and 10.64% on partly cloudy days. All the studies mentioned so far report interesting results; however, none of them discusses the tracking accuracy achieved by the systems.

In this context, the present work introduces the development and evaluation of a two-axis active solar tracking system applied to a CSP. The system was experimentally tested under real operating conditions over a period of 10 days, demonstrating excellent accuracy and a significantly higher capture of direct normal irradiance (DNI) compared to global horizontal irradiance (GHI). The system was developed at the Federal Institute of Paraíba – Cajazeiras Campus, Brazil, as part of an ongoing research project that employs the solar concentrator for water distillation.

Figure 1 shows the CSP used in this study, prior to the installation of any instrumentation and control system. The CSP features two movement axes (azimuth and zenith) and a diameter of 1.35 meters. The motors coupled to the axes are Bosch direct current (DC) motors, adapted from truck windshield wipers. These motors incorporate mechanical reduction through a pinion–worm gear system. In addition, the CSP is equipped with gear rings on each axis, allowing high torque for system movement.

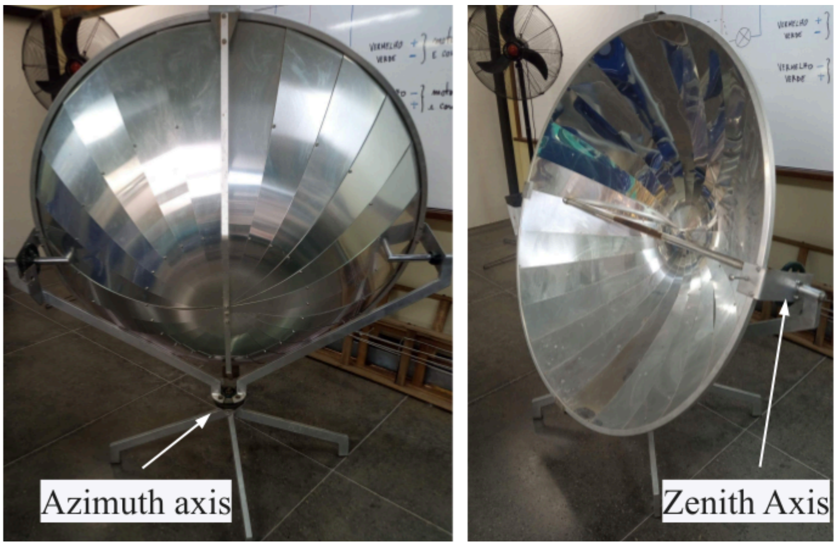

Figure 1. CSP used in this study

2. Methodology

2.1 Sensing

The sensing system adopts a configuration similar to that described by Dadi and Peravali (2020) and Ayoade et al., (2022), based on detecting the solar position through variations in illumination and shading on photosensitive sensors. The arrangement consists of light-dependent resistors (LDRs) placed side by side and separated by a physical barrier, as illustrated in Figure 2. The operating principle relies on the analog reading of the LDRs and the light difference caused by the barrier. This variation is used to identify misalignment relative to the Sun's position, enabling fine adjustment of the tracking system.

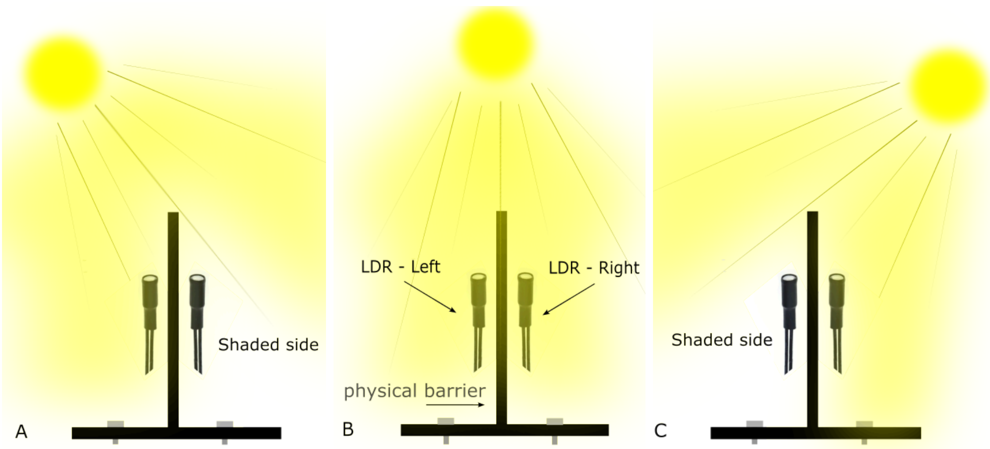

Figure 2. Schematic representation of LDR sensors used for each movement axis (azimuth and solar elevation). (A) Sunlight on the left side of the sensor. (B) Sunlight aligned with the sensor. (C) Sunlight on the right side of the sensor.

As illustrated in Figure 2-A, the physical barrier positioned between the LDRs casts a shadow over the right-hand sensor. Under this condition, the electric actuator is activated to rotate the system counterclockwise until the difference between the analog readings of the sensors falls within a predefined tolerance margin. In Figure 2-B, the readings are within this margin, indicating that the system is aligned with the Sun's position, and no motor action is required. In Figure 2-C, the shadow falls on the left-hand LDR, and the actuator must rotate the system clockwise to restore alignment. This sensing arrangement is employed for each axis of the system: azimuth and solar elevation.

2.2 Automatic Tracking Algorithm

Figure 3 presents the flowchart of the algorithm implemented on the Arduino for controlling the solar tracking system. The process begins with the definition of pins and control variables, followed by the configuration of inputs and outputs. Next, the rampPWM function is declared as a global function, allowing it to be called at any moment within the main program loop. This function plays a crucial role by actuating the motors progressively, applying acceleration and/or deceleration ramps to smooth the system's movement. Additional details regarding its implementation are presented in Section 2.2.1.

Next, the system performs the analog reading of the LDRLeft and LDRRight sensors, calculates the difference between their values, and stores the result in the variable *D*. After obtaining the difference (*D)*, the value is compared with a constant called the tolerance margin (*TM*). This comparison determines the direction in which the motor will be actuated and sets a minimum threshold for motor activation, preventing unnecessary movements when the illumination difference between the sensors is small.

In this way, the tolerance margin (*TM*) functions as an adjustable hysteresis, allowing control over the system's sensitivity. The smaller the *TM* value, the higher the sensor sensitivity and, consequently, the more frequent the motor activation.

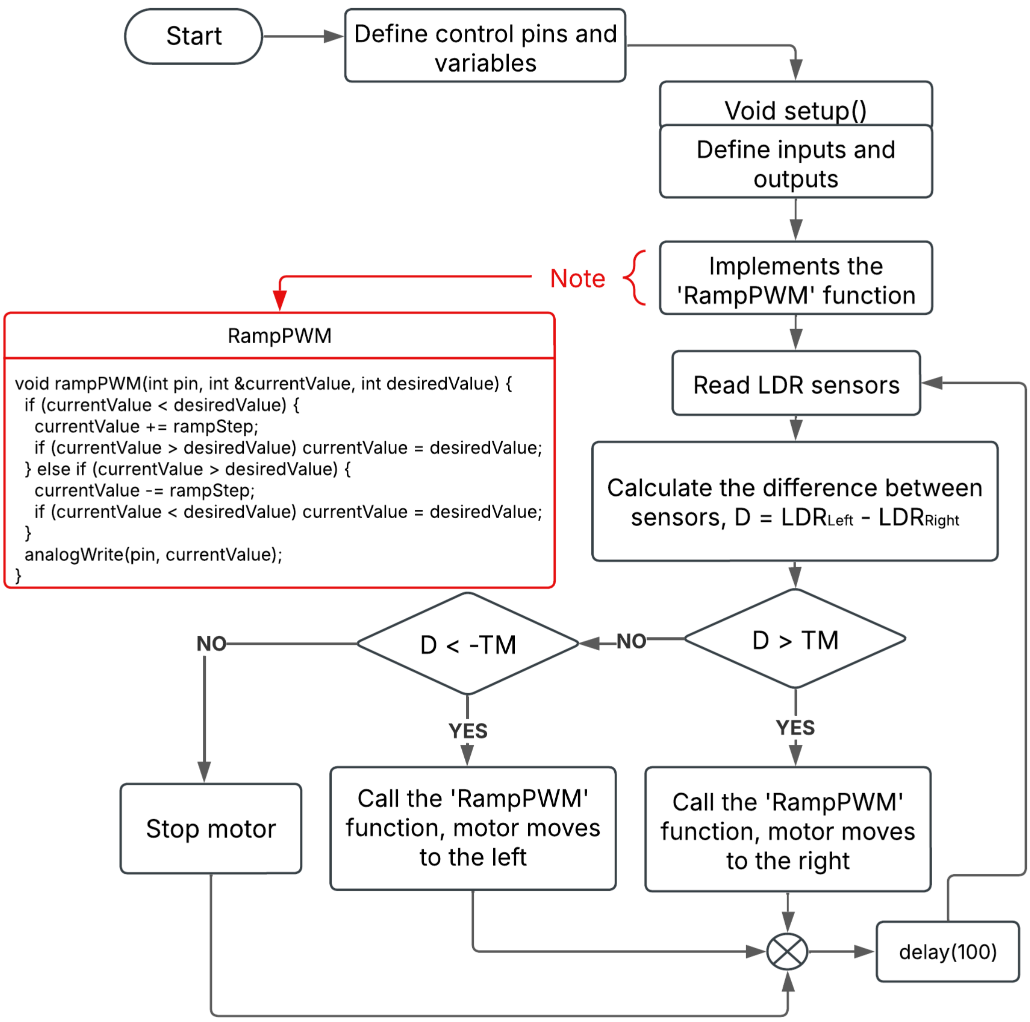

Figure 3. Flowchart of the automatic tracking system

As indicated in the flowchart, motor control occurs under the following conditions: If $D > TM$, there is an imbalance in illumination, indicating that the concentrator should move to the right. In this case, the *rampPWM()* function is called to progressively actuate the motor in that direction. If $D < -TM$, the system detects that the concentrator needs to be adjusted to the left, activating the *rampPWM()* function to move it accordingly. If the reading difference is within the tolerance range ($-TM < D < TM$), the motor remains off, as the system considers the concentrator alignment to be adequate. This logic is applied to both axes of the solar tracking system.

2.2.1 Function *rampPWM*

The *rampPWM* function was developed to regulate the acceleration and deceleration of the motors progressively, aiming to reduce mechanical stress and prevent structural oscillations during the repositioning of the solar tracker. Its operating principle is based on the application of pulse-width modulation (PWM) with gradual variation of the output value. To achieve this, the function continuously compares the current PWM value (*currentValue*) with the desired value (*desiredValue*), adjusting it in fixed increments or decrements (*rampStep*) until the target value is reached.

When *currentValue* < *desiredValue*, the signal is progressively increased; when *currentValue* > *desiredValue*, the signal is gradually decreased. This control prevents abrupt transitions, ensuring that mechanical movement occurs smoothly. Moreover, this control strategy minimizes issues such as overshoot, a problem reported in systems operating with purely on-off control (Queiroz et al., 2020). Figure 4 shows the implemented *rampPWM* function.

```
// Function: rampPWM
// Purpose: Gradually adjust the PWM signal applied to a motor (or other device)
//          so that it accelerates or decelerates smoothly toward the desired value.
void rampPWM(int pin, int &currentValue, int desiredValue) {

  // If the current PWM value is less than the target,
  // increase it gradually by "rampStep"
  if (currentValue < desiredValue) {
    currentValue += rampStep;
    // Ensure it does not exceed the desired value
    if (currentValue > desiredValue)
      currentValue = desiredValue;
  }

  // If the current PWM value is greater than the target,
  // decrease it gradually by "rampStep"
  else if (currentValue > desiredValue) {
    currentValue -= rampStep;
    // Ensure it does not drop below the desired value
    if (currentValue < desiredValue)
      currentValue = desiredValue;
  }
  // Apply the updated PWM value to the specified pin
  analogWrite(pin, currentValue);
}
```

Figure 4. Implementation of the *rampPWM* function

The function has three arguments that operate as input parameters (*int pin*, *int &currentValue*, *int desiredValue*).

- *int pin*: the Arduino pin number that will generate the PWM signal. This pin may change depending on which motor is to be actuated and in which rotation direction.
- *int currentValue*: the current PWM value applied to the motor.
- *int desiredValue*: the target PWM value to be reached (this parameter is defined as a constant and represents the maximum PWM value applied to the motor, ranging from 0 to 255).

Additionally:

- *rampStep*: the increment step for motor acceleration or deceleration, defined in the program as *rampStep = 5*.
- *analogWrite(pin, currentValue)*: updates the PWM applied to the motor.

The function logic operates as follows: if *currentValue* is less than *desiredValue*, it is incremented by the amount defined in *rampStep*. If *currentValue* is greater than *desiredValue*, it is gradually decremented by the same step. This process ensures that the motor does not experience abrupt speed changes. When *currentValue* reaches *desiredValue*, the ramp is stopped. It is important to highlight that two BTS7960 power drivers were used, responsible for receiving the PWM signals from the Arduino and performing the switching to the motors.

2.3 Accuracy Measurement

To evaluate the system's accuracy, the Instantaneous Solar Tracking Error (ISTE) was measured, defined as the actual angular difference between the direction of direct solar radiation and the position to which the solar tracker is oriented (Angulo-Calderón et al., 2022).

The ISTE determination was carried out using a simple apparatus developed based on the operating principle of a gnomon. The term *gnomon*, of Greek origin, refers to a rod that casts its shadow onto a plane and has historically been used for time measurement (Batista et al., 2025).

Figure 5-A shows the gnomon constructed for this study, in which the distance between the centroids of each concentric circle is 5 mm, while the x and y axes have graduations with 1 mm spacing. Figure 5-B illustrates details of the procedure adopted for reading the measurements obtained with the instrument.

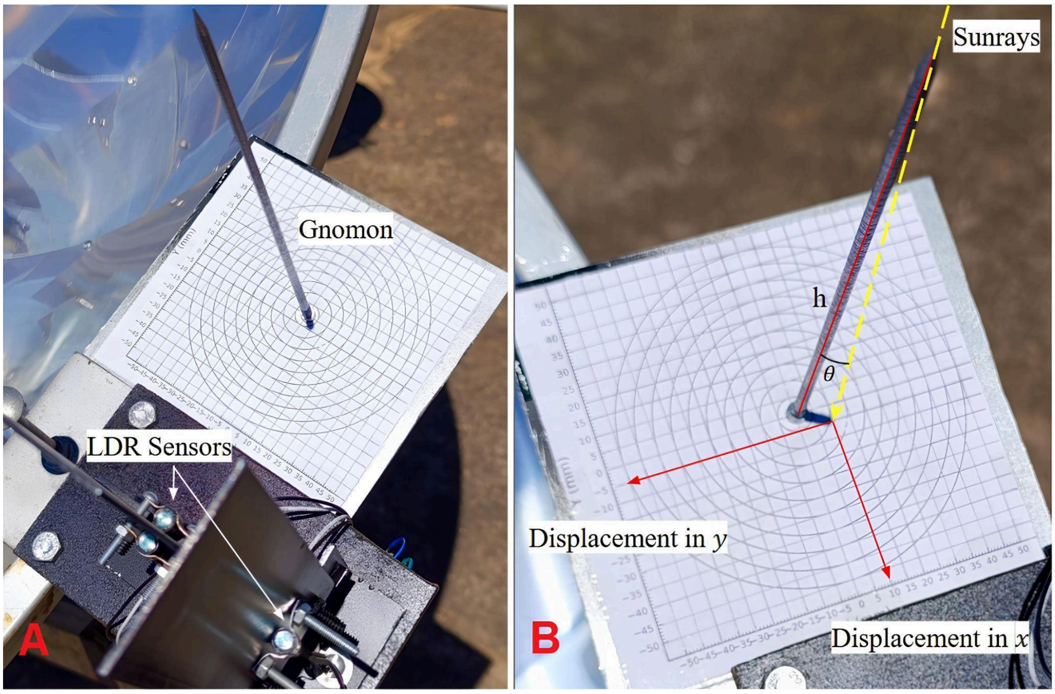

Figure 5. Apparatus for measuring the Instantaneous Solar Tracking Error (ISTE)

The instrument was mounted on the face of the CSP. Angular deviations in the azimuth axis (α), zenith axis (β), and the instantaneous tracking error – ISTE (θ) – are determined from Equations 1, 2, and 3 (Angulo-Calderón et al., 2022), respectively. The term h refers to the length of the rod, which in this study was 300 mm. The variables x and y correspond to the projections, in the Cartesian plane, of the distance between the centroid of the solar ray projections and the center of the concentric circles.

The shadow cast by the rod onto the plane represents the magnitude of the vector v, which is inclined at an angle θ, as observed in Figure 5-B. This angle θ, calculated using Equation 3, corresponds to the Instantaneous Solar Tracking Error (ISTE).

$$\alpha = \arctan (x / h) \qquad \text{(eq. 1)}$$

$$\beta = \arctan (y / h) \qquad \text{(eq. 2)}$$

$$\theta = \arctan (v / h) = \arctan \sqrt{x^2 + y^2} / \mathrm{h} \qquad \text{(eq. 3)}$$

2.4 Measurement of GHI and DNI

To evaluate the performance of the tracking system, the Direct Normal Irradiance (DNI) measured on the face of the CSP was compared with the Global Horizontal Irradiance (GHI). Direct Normal Irradiance (DNI) refers to the amount of direct solar radiation striking a surface perpendicular to the solar rays, whereas Global Horizontal Irradiance (GHI) refers to the total amount of radiation incident on a fixed horizontal surface (Kalogirou, 2016; NREL, 2025). In this study, two portable radiation sensors from Instrutherm, model MES-100, were used. Figure 6 shows the location of the instruments, as well as details of the LDR sensors and motors.

Figure 6. Details of the location of DNI and GHI radiation sensors, LDR sensors, and electric motors.

The MES-100 sensor mounted on the horizontal plane is responsible for measuring the Global Horizontal Irradiance (GHI). Meanwhile, the MES-100 attached to the face of the solar concentrator follows the apparent movement of the Sun, measuring the direct irradiance incident perpendicular to the concentrator surface, i.e., the Direct Normal Irradiance (DNI). The values obtained from both instruments are compared in order to quantify the performance of the solar tracker in capturing solar radiation.

The tracking system was evaluated at the facilities of the Federal Institute of Paraíba, Cajazeiras Campus, Brazil (latitude -6.8892; longitude -38.5451). Ten experiments were conducted from 6:00 a.m. to 6:00 p.m., with measurements of DNI and GHI sensors taken every hour. Accuracy measurements (ISTE) were also performed on an hourly basis.

3. Results and Discussion

3.1 Response of LDR Sensors and Actuators

Initially, the tracking system was tested in the laboratory to evaluate the response of the sensors and actuators. For this purpose, tests were conducted by illuminating the LDRs with a spotlight and recording the response of both sensors and actuators. The graphs in Figure 7 show the system behavior for the azimuth axis when the spotlight is moved from right to left. Note: The graphs should be interpreted at the same time instant.

Between seconds 1 and 6: The graphs show that the LDR sensors are initially aligned with the light source, as the reading difference between the sensors is within the tolerance margin, as observed in Figure 7-B. This margin was previously set in the algorithm as ±50. Therefore, between 1 and 6 seconds, the motor does not receive a PWM signal, as can be seen in Figure 7-C.

Between seconds 7 and 13: A significant difference is observed in the analog readings of the LDR sensors (Figure 7-B), indicating a system misalignment. This triggers a corrective reaction, as evidenced by the PWM signal applied to the motor (Figure 7-C).

Between seconds 13 and 16: The concentrator momentarily exceeds the ideal alignment point with the light source (minor overshoot). This behavior can be identified at the crossing of the analog readings (Figure 7-A). In response, the system applies a slight reversal to the motor rotation direction (*PWM Left*), as observed in Figure 7-C, ensuring fine adjustment of the position.

Between seconds 17 and 22: The system is fully aligned with the light source, which can be observed from the stabilization of the sensor analog values (Figure 7-A) and from the difference (*D*) remaining within the ±50 limits (Figure 7-B).

Finally, as observed in the graph in Figure 7-C, the PWM signal exhibits a ramp-like behavior during both motor acceleration and deceleration, ensuring smooth movements of the system's mechanical structure

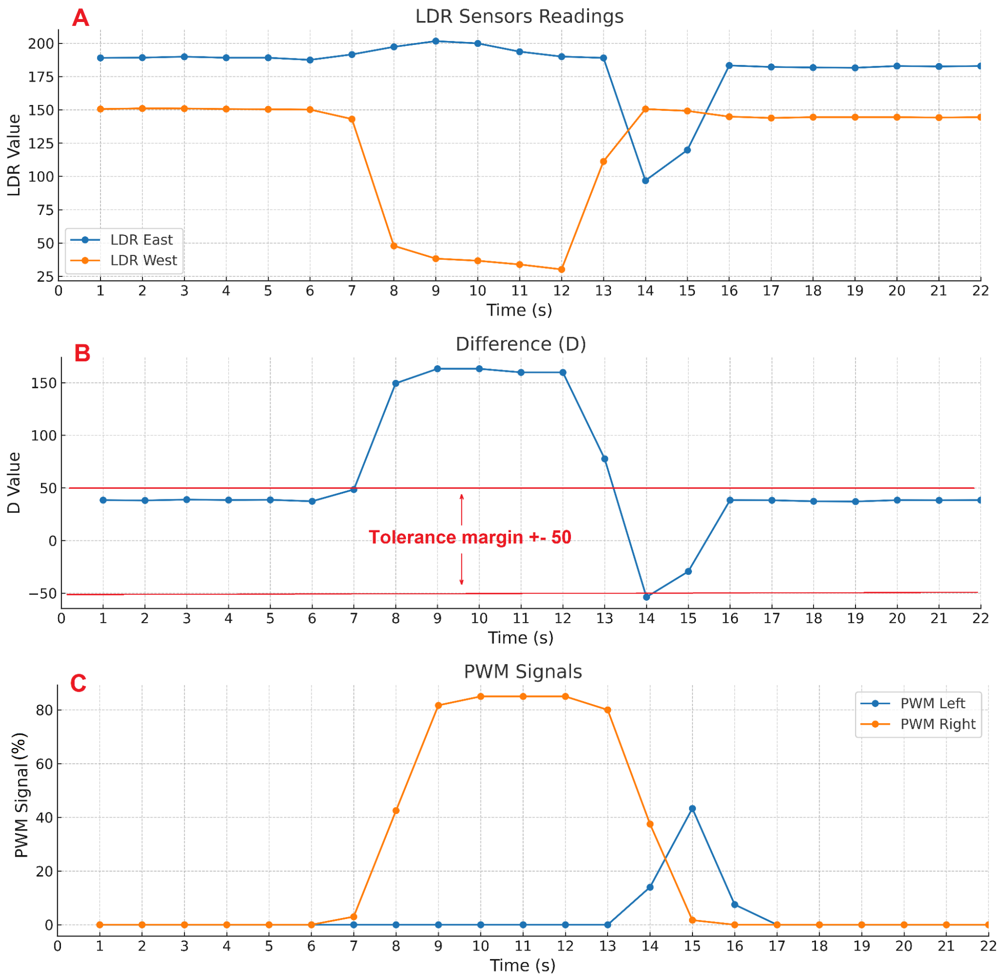

Figure 7. Response of sensors and actuator for the azimuth axis

3.2 DNI and GHI Results

For analysis and comparison purposes, the measurement days were classified into two categories: "partly cloudy day," when the daily Global Horizontal Irradiance (GHI) was up to 500 W/m²·day, and "sunny day," when the daily GHI exceeded 501 W/m²·day.

Table 1 presents the values of Direct Normal Irradiance (DNI) and Global Horizontal Irradiance (GHI) at the end of each test day. As expected, in all cases, the DNI measured on the face of the solar concentrator exceeded the GHI. This result is a consequence of the two-axis solar tracking system, which keeps the MES-100 sensor continuously aligned with the Sun's apparent movement, maximizing the capture of direct radiation..

On sunny days (03/July, 01/August, 07/August, 08/August, and 14/August), the DNI values were significantly high, all exceeding 730 W/m²·day, reaching 859.8 W/m²·day on 14/August. This performance is explained by the tracking system, which kept the sensor always perpendicular to the solar rays, thereby recording the maximum available direct radiation. On the other hand, the GHI, being fixed on the horizontal plane, showed lower values since the projection of the solar beam onto this plane depends on the incidence angle and only accounts for the diffuse fraction of the radiation. For these days, the relative difference between DNI and GHI was considerable, ranging from 47% to 64%, highlighting the importance of Sun alignment under clear-sky conditions.

On days classified as partly cloudy (30 June, 09 July, 10 July, 12 July, and 20 July), although the DNI remained higher than the GHI, the percentage difference between them was reduced. Notably, on 30 June, the tracker's gain was only 14.56%. This behavior is explained by the presence of clouds, which attenuate the direct component of solar radiation and enhance its diffuse component, thereby reducing the benefit of tracking compared to the horizontal plane.

Table 1. Results of Direct Normal Irradiance (DNI) and Global Horizontal Irradiance (GHI) measurements

Day	DNI (W/m².dia)	GHI (W/m².dia)	Variation (%)	Climatic condition
30/06/2025	357,2	311,8	14,56	Partly cloudy day
03/07/2025	800,4	489,4	63,55	Sunny day
09/07/2025	478,8	382,7	25,11	Partly cloudy day
10/07/2025	489,6	350,9	39,53	Partly cloudy day
12/07/2025	453,2	373,2	21,44	Partly cloudy day
20/07/2025	662,2	444,2	49,08	Partly cloudy day
01/08/2025	736,7	500,9	47,08	Sunny day
07/08/2025	838,9	545,4	53,81	Sunny day
08/08/2025	834,5	548,0	52,28	Sunny day
14/08/2025	859,8	562,3	52,91	Sunny day

Figure 8 presents, in detail and on an hourly scale, the energy measured by the DNI and GHI sensors over a sunny day and a partly cloudy day. It can be observed that the effect of solar tracking is more pronounced under clear-sky conditions, particularly during the early morning hours (6:00–9:00) and late afternoon (15:00–18:00), when the difference between DNI and GHI becomes more significant.

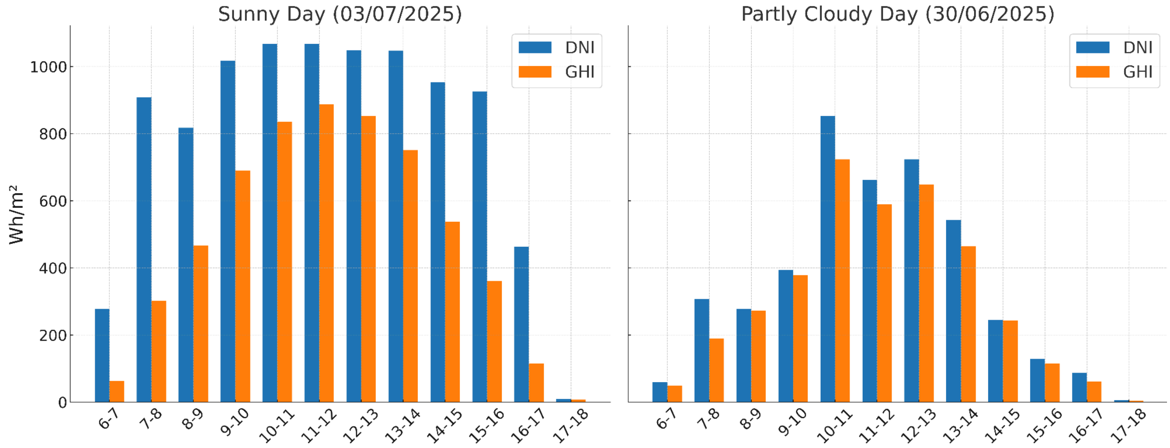

Figure 8. Hourly DNI and GHI results for 03 July 2025 (Sunny) and 30 June 2025 (Partly Cloudy)

In contrast, for the partly cloudy day, the graph shows a reduced effect of the solar tracker. It can be observed that during intervals such as 08:00–09:00, 09:00–10:00, 14:00–15:00, and 15:00–16:00, the DNI and GHI values were very close. This behavior confirms that during periods dominated by clouds, the effectiveness of solar tracking is significantly diminished.

3.3 Instantaneous Solar Tracking Error - ISTE

Table 2 presents the average daily error, obtained from the average of all instantaneous errors recorded between 8:00 AM and 4:00 PM. On partly cloudy days, it was not possible to accurately determine the tracking system's accuracy because, at certain times, the presence of clouds prevented the gnomon's rod from casting a shadow on the Cartesian plane, compromising accurate measurement. In the table, the abbreviation "N.d" stands for not determined.

Table 2: Average tracking error for the test days Between 8am and 4pm

Day	Average ISTE – Values in Degrees (°)	Climatic condition
30/06/2025	N.d	Partly cloudy day
03/07/2025	1,98°	Sunny day
09/07/2025	N.d	Partly cloudy day
10/07/2025	N.d	Partly cloudy day
12/07/2025	N.d	Partly cloudy day
20/07/2025	N.d	Partly cloudy day
01/08/2025	1,84°	Sunny day
07/08/2025	2,02°	Sunny day
08/08/2025	2,37°	Sunny day
14/08/2025	2,09°	Sunny day

Figure 9 shows the variation of the ISTE for 03 July 2025 (sunny day). It can be observed that at 07:00 and 17:00, there is a large misalignment of the system relative to the Y-axis, resulting in ISTE values of 6.99° and 9.47°, respectively. This behavior is due to the mechanical travel limitations of the solar concentrator system: at 07:00 and 17:00, the Sun is at an elevation that the tracker cannot reach because of the end-of-travel constraints of the mechanism. Considering only the hours between 08:00 and 16:00, the maximum instantaneous error measured was 2.64° (13:00), while the average ISTE was 1.98°, demonstrating the good accuracy of the developed tracking system.

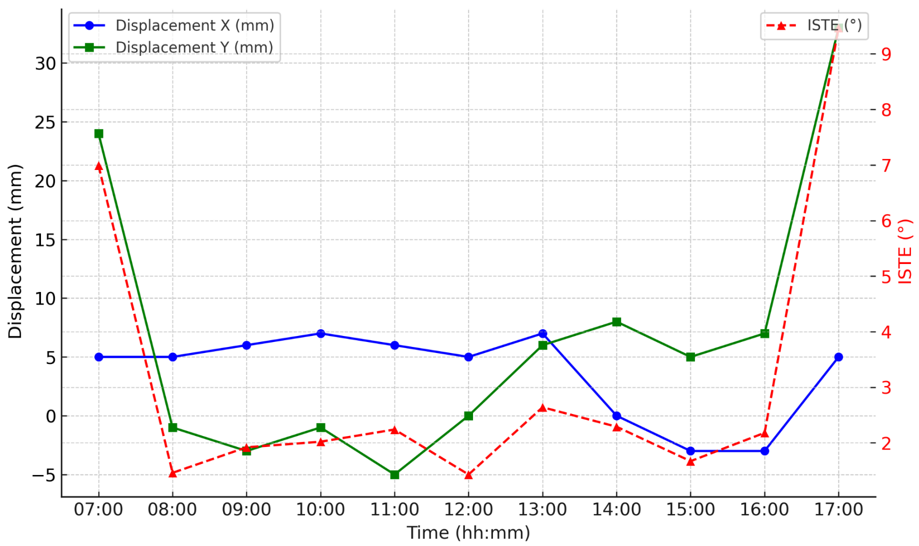

Figure 9. Variation of the Instantaneous Solar Tracking Error (ISTE) for 03 July 2025

The graph in Figure 10 shows the tracking precision results for 30 June 2025 (partly cloudy day). On this day, the significant presence of clouds compromised ISTE measurements at certain times, such as 07:00, 08:00, 11:00, 14:00, 15:00, 16:00, and 17:00.

Although the ISTE could not be determined at specific times, it is important to note that the tracking system logic was designed to operate based on the illumination and shading of the LDR sensors. Thus, when the sky is cloudy or clouds pass sporadically, the tracking mechanism maintains its position until the Sun reappears. This feature is advantageous because it ensures that the tracker remains minimally aligned with the Sun's direction, even in the presence of clouds.

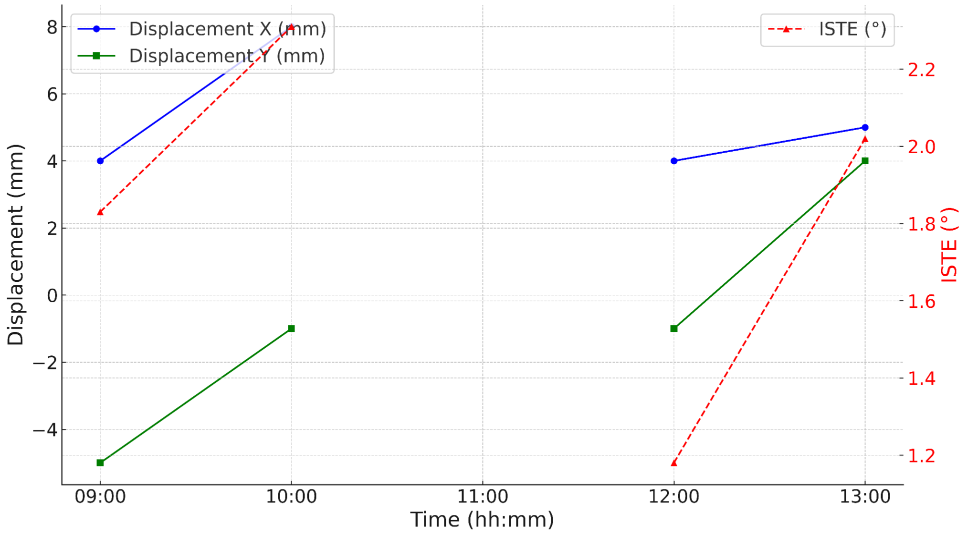

Figure 10. Variation of the Instantaneous Solar Tracking Error (ISTE) for 30 June 2025

4. Conclusion

The developed tracking system demonstrated high performance and robustness, ensuring continuous alignment of the solar concentrator's surface with the Sun's position. The RampPWM control function enabled smooth and progressive motor actuation, both during acceleration and deceleration, minimizing abrupt movements of the CSP's mechanical structure and consequently reducing wear on electrical and mechanical components.

The tracker was subjected to experimental tests under real operating conditions. The results showed that the DNI measured on the CSP surface was significantly higher than the GHI on sunny days, and slightly higher on partly cloudy days, confirming the system's effectiveness in maximizing direct solar energy capture.

The tracking accuracy was evaluated through the Instantaneous Solar Tracking Error (ISTE), determined at hourly intervals. For the five sunny days analyzed, the average accuracy between 08:00 and 16:00 was 1.98°, 1.84°, 2.02°, 2.37°, and 2.09°, respectively. The maximum recorded ISTE was 2.86°. However, it should be emphasized that the use of a gnomon does not allow for precise determination of the pointing error during periods of cloud cover, in such cases, alternative methods can be employed, such as the use of absolute encoders installed on the motor shafts to compare the actual position with the solar position calculated through solar position equations. Nevertheless, this method entails higher costs.

Additionally, the mechanical system presented minor play in the azimuth and zenith axes, suggesting opportunities to improve precision through adjustment of these components. Future work may include:

- Measurement of electrical energy consumption to evaluate the performance of the electronic system and actuators;
- Development of an electronic gnomon capable of continuously calculating ISTE;
- Installation of a small photovoltaic module dedicated to powering the tracker's electronic system.

Referências

Angulo-Calderón, M. Salgado-Tránsito, I. Trejo-Zúñiga, I. Paredes-Orta, C. Kesthkar, S. Díaz-Ponce, A. , 2022. Development and Accuracy Assessment of a High-Precision Dual-Axis Pre-Commercial Solar Tracker for Concentrating Photovoltaic Modules. Appl. Sci. 2022, 12, 2625

Al-Saadi, Y.R. Tapu, M.S. Bidi, A.A. Abdulla, S. Diykh,M., 2022. Developing Smart Self Orienting Solar Tracker for Mobile PV Power Generation Systems. in IEEE Access, vol. 10, pp. 79090-79099.

Ayoade, I. A. Adeyemi, O. A. Adeaga, O. A. Rufai, R. O. and Olalere, S. B., 2022. Development of Smart (Light Dependent Resistor, LDR) Automatic Solar Tracker. IEEE 5th Information Technology for Education and Development (ITED).

Batista, M.C. Sanches, Y.Y.R. Santos, O.R. Sitko, C.M. Vieira, T.F. Ferreira, M., 2025. Fundamentos e Metodologia de Construção de um Relógio Solar Analemático para o Ensino de Astronomia. [in Portuguese]. Brazilian Journal of Physics Teaching, vol. 47, e20250213 (2025). DOI: https://doi.org/10.1590/1806-9126-RBEF-2025-0213

Dadi, V., Peravali, S., 2020. Optimization of light-dependent resistor sensor for the application of solar energy tracking system.© Springer Nature Switzerland AG 2020. SN Appl. Sci. 2, 1499 .

Elsayed, A.A. Khalil, E.E. Kassem, M.A. Huzzayin, O.A., 2021. A novel mechanical solar tracking mechanism with single axis of tracking for developing countries. Renewable Energy. Volume 170, June 2021, Pages 1129-1142

Hammoumi, A.E. Chtita, S. Motahir, S. Ghzizal, A.E., 2022. Solar PV energy: From material to use, and the most commonly used techniques to maximize the power output of PV systems: A focus on solar trackers and floating solar panels. Energy Reports, Volume 8, November 2022, Pages 11992-12010.

National Renewable Energy Laboratory., 2025. *Solar glossary*. U.S. Department of Energy. Available in : https://www.nrel.gov/grid/solar-resource/solar-glossary.html. Access on july 15, 2025.

Queiroz, J.R. Souza, A, S. Gussoli, M. K. Oliveira, J.C.D. Andrade, C.M.G., 2020. Construction and Automation of a Microcontrolled Solar Tracker. processes 2020, 8, 1309. https://doi.org/10.3390/pr8101309

Stanek, B. Wecel, D. Bartela, L. Rulik, S., 2022. Solar tracker error impact on linear absorbers efficiency in parabolic trough collector – Optical and thermodynamic study. Renewable Energy, Volume 196, August 2022, Pages 598-609

Saeedi, M. Effatnejad, R., 2021. A New Design of Dual-Axis Solar Tracking System With LDR Sensors by Using the Wheatstone Bridge Circuit. in IEEE Sensors Journal, vol. 21, no. 13, pp. 14915-14922

Sun, L. Bai, J. Pachauri, R.K. Wang,S., 2024. A horizontal single-axis tracking bracket with an adjustable tilt angle and its adaptive real-time tracking system for bifacial PV modules. Renewable Energy. Volume 221, February 2024, 119762

Sousa, M.D. Abreu, W.G. Alves, J.L., 2022. Desenvolvimento e análise do ganho energético líquido de um rastreador solar de eixo único conectado à rede elétrica [in Portuguese].Journal of Engineering and Technology. V.14, july. Pg 253-264. Available in : https://revistas.uepg.br/index.php/ret/article/view/20233/209209216706

KALOGIROU, S. A, 2016. Engenharia de energia solar, processos e sistemas. [in Portuguese] 2. ed. Rio de Janeiro: Elsevier, 2016. 843 p.

Kuttybay, N. Mekhilef, S. Kashkarbay, N. Saymbetov, A. Nurgaliyev, M. Dosymbetova, G. Orynbassar, S. Yershov, E. Kapparova, A. Zholamanov, B. Bolatbek, A., 2024. Assessment of solar tracking systems: A comprehensive review. Sustainable Energy Technologies and Assessments. Volume 68, August 2024, 103879